Cancer Letters 467 (2019) 58–71

Contents lists available at ScienceDirect

Cancer Letters

journal homepage: www.elsevier.com/locate/canlet

Original Articles

# MLKL contributes to shikonin-induced glioma cell necroptosis via promotion of chromatinolysis

Ye Ding[a,b], Chuan He[a,b], Shan Lu[a,b], Xuanzhong Wang[a,b], Chongcheng Wang[a,b], Lei Wang[a,b], Ji Zhang[c], Meihua Piao[d], Guangfan Chi[e], Yinan Luo[a,b], Ke Sai[c,**], Pengfei Ge[a,b,*]

[a] Department of Neurosurgery, First Hospital of Jilin University, Changchun, 130021, China
[b] Research Center of Neuroscience, First Hospital of Jilin University, Changchun, 130021, China
[c] Department of Neurosurgery, Sun Yat-sen University Cancer Center, State Key Laboratory of Oncology in South China, Collaborative Innovation Center for Cancer Medicine, Guangzhou, 510060, China
[d] Department of Anesthesiology, First Hospital of Jilin University, Changchun, 130021, China
[e] Key Laboratory of Pathobiology, Ministry of Education, Jilin University, Changchun, 130021, China

ARTICLE INFO

*Keywords:*
MLKL
Chromatinolysis
Necroptosis
Glioma
Shikonin

ABSTRACT

Chromatinolysis refers to enzymatic degradation of nuclear DNA and is regarded as one of the crucial events leading to cell death. Mixed-lineage kinase domain-like protein (MLKL) has been identified as a key executor of necroptosis, but it remains unclear whether MLKL contributes to necroptosis via regulation of chromatinolysis. In this study, we find that shikonin induces MLKL activation and chromatinolysis in glioma cells in vitro and in vivo, which are accompanied with nuclear translocation of AIF and γ-H2AX formation. In vitro studies reveal that inhibition of MLKL with its specific inhibitor NSA or knockdown of MLKL with siRNA abrogates shikonin-induced glioma cell necroptosis, as well as chromatinolysis. Mechanistically, activated MLKL targets mitochondria and triggers excessive generation of mitochondrial superoxide, which promotes AIF translocation into nucleus via causing mitochondrial depolarization and aggravates γ-H2AX formation via improving intracellular accumulation of ROS. Inhibition of nuclear level of AIF by knockdown of AIF with siRNA or mitigation of γ-H2AX formation by suppressing ROS with antioxidant NAC effectively prevents shikonin-induced chromatinolysis. Then, we found that RIP3 accounts for shikonin-induced activation of MLKL, and activated MLKL reversely up-regulates the protein level of CYLD and promotes the activation of RIP1 and RIP3. Taken together, our data suggest that MLKL contributes to shikonin-induced glioma cell necroptosis via promotion of chromatinolysis, and shikonin induces a positive feedback between MLKL and its upstream signals RIP1 and RIP3.

## 1. Introduction

Mixed-lineage kinase domain-like protein (MLKL) has been identified as a key executor of necroptosis, which is a new type of programmed cell death with morphological similarities to necrosis [1–3]. After being recruited to necrosome complex consisting mainly of receptor interacting serine-threonine protein kinases 1 (RIP1) and 3 (RIP3), MLKL is phosphorylated by RIP3 at T357 and S358 and then activated [1]. When the activated MLKL forms homotrimer, it produced multiple biological effects such as disrupting cell membrane, inducing cation channels in plasma membrane and triggering formation of NLRP3 inflammasome [1–6]. However, it is still unclear whether activated MLKL could lead to other biological effects during the process of necroptosis.

DNA is one of the most essential molecules in eukaryotic cells and contains all the information necessary for maintaining cellular physiological functions [7]. Chromatinolysis refers to enzymatic degradation of nuclear DNA [8]. Proper degradation of DNA could prevent disease occurrence. However, excessive degradation of DNA makes cell death program irreversible and facilitates nucleus disassembly, and thus is regarded as one of the key events leading to cell death [7]. Chromatinolysis has been studied extensively in the case of apoptosis. It was found that DNA is cleaved into large fragments (50–200 kb), then cleaved into nucleosomal units (180 bp) and finally degraded into oligonucleotides or smaller molecule by deoxyribonuclease (DNase) [9]. Although less is known about the factors or mechanisms responsible for

* Corresponding author. Department of Neurosurgery, First Hospital, Jilin University, 71 Xinmin Avenue, Changchun, 130021, Jilin Province, China.
** Corresponding author.
*E-mail addresses:* saike@sysucc.org.cn (K. Sai), drgepengfei@163.com, pengfeige@gmail.com (P. Ge).

https://doi.org/10.1016/j.canlet.2019.09.007
Received 15 July 2019; Received in revised form 16 September 2019; Accepted 17 September 2019

chromatinolysis in necroptosis, accumulating evidences have shown that nuclear translocation of apoptosis inducing factor (AIF) from mitochondria and γ-H2AX formation contributed to chromatinolysis in necroptotic cells [7,10].

Shikonin is a naphthoquinone isolated from Lithospermum erythrorhizon. It exerted therapeutic effect on various types of cancers such as glioma, osteosarcoma, breast cancer, colon cancer and multiple myeloma via activation of necroptosis pathway [11–15]. RIP1 and RIP3 were both reported to contribute to shikonin-induced glioma cell necroptosis [11], but in which the role of MLKL remains elusive. In our previous study, we found that the nuclei in shikonin-treated glioma cells were electron-lucent under transmission electronic microscope [16], indicating induction of chromatinolysis might be a pathway via which shikonin triggered glioma cell necroptosis. Therefore, we investigated in this study whether MLKL is involved in shikonin-induced glioma cell necroptosis and its role in regulation of chromatinolysis.

## 2. Materials and methods

### 2.1. Reagents

Shikonin, NAC (N-Acetyl Cysteine), and MnTBAP (metalloporphyrin Mn (III) tetrakis (4-benzoic acid) porphyrin) were all purchased from Sigma (St.Louis, MO). NSA (Necrosulfonamide) was from Selleckchem company (Houston, TX). Shikonin was dissolved in PBS to a storage concentration of 50 mmol/L. Anti-RIP1, anti-RIP3, *anti*-phospho-RIP3 at Ser227, *anti*-H2A antibodies were purchased from Abcam company (Cambridge, MA). *Anti*-phospho-RIP1at Ser166 antibody was from cell signaling company (Danvers, MA). *Anti*-β-Actin antibody was from Santa Cruz Biotechnology (Santa Cruz, CA). Other reagents were purchased from Sigma (St. Louis, MO).

### 2.2. Cell line and culture

Human SHG-44, U87 and U251 and rat C6 glioma cells were all obtained from Shanghai Institute of Cell Biology, Chinese Academy of Sciences (Shanghai, China). They were cultured in DMEM supplemented with 10% fetal bovine serum, 2 mmol/L glutamine, penicillin (100 U/mL) and streptomycin (100 μg/mL), and maintained at 37 °C and 5% $CO_2$ in a humid environment. Cells in the mid-log phase were used in the experiments.

### 2.3. Lactate dehydrogenase release cell death assay

The cells were seeded onto 96-well microplate and cultured 24 h. Lactate dehydrogenase cytotoxicity assay kit (Beyotime Biotech, Nanjing, China) was used to assay cellular death rate. According to the manufacturer's instructions, the absorbance value of each sample was read at 490 nm, and cell death ratio was calculated by using the following formula: cell death ratio % = (A sample – A control/A max – A control) × 100. A sample: sample absorbance value; A control: the absorbance value of control group; A max: the absorbance value of positive group.

### 2.4. Assessment of necrosis by flow cytometry

SHG-44 and U251 glioma cells were collected and then the Annexin V-FITC detection kit (Invitrogen, Grand Island, NY) was used for assessment of cell death modality as described by the manufacture's instruction. The collected cells were washed twice with PBS, and resuspended in 400 μL 1 × binding buffer, and then transferred to a 5-mL culture tube containing 5 μL of annexin V-FITC and 10 μL of propidium iodide. After incubation for 15 min at room temperature in the dark, 1 × binding buffer was added into each tube and the stained cells were analyzed by flow cytometry (FACScan, Becton Dickinson, San Jose, CA). The rate of cell death was analyzed using CELLquest software (Becton Dickinson). Data acquisition was conducted by collecting 20,000 cells per tube and the numbers of viable and dead cells were determined for each experimental condition.

### 2.5. Mitochondrial membrane potential assay

The SHG-44 and U251 glioma cells were collected and stained with JC-1 according to manufacturer's instruction (Beyotime Biotech, Nanjing, China). Then, the ells were analyzed by flow cytometry (FACScan, Becton Dickinson, San Jose, CA).

Another group of SHG-44 cells seeded onto a culture dish with a diameter of 3 cm were treated as the same as above described, and then observed under fluorescence microscope (Olympus IX71, Tokyo, Japan).

### 2.6. Measurement of mitochondrial superoxide

Mitochondrial superoxide was assayed by using MitoSOX red (Invitrogen company, Eugene, OR) as described by manufacture's instruction. The SHG-44 cells seeded onto 96-well microplate were incubated 10min with 2.0 mL MitoSOX reagent working solution at 5 μmol/L at 37 °C in dark, and then washed with PBS. The red fluorescence density was measured at an excitation wavelength of 510 nm and an emission wavelength at 580 nm, and was expressed as a ratio to the fluorescence in control cells.

Another group of SHG-44 glioma cells seeded onto a culture dish with a diameter of 3 cm were treated as described above, and observed under fluorescence microscope (Olympus IX71, Tokyo, Japan).

### 2.7. Transfection of small interfering RNA (siRNA)

SHG-44 ($15 \times 10^5$ cells/ml) and U251 ($15 \times 10^5$ cells/ml) cells were seeded onto a culture dish in a diameter of 10 cm. Transfection of siRNA was performed by using Lipofectamine 2000 (Invitrogen, USA) according to the manufacturer's instructions.

The MLKL siRNA (5′- CCUCUGUGGAUGAAAUCUUTT-3′), AIF SiRNA (5′-GCAGUGGCAAGUUACUUAUTT-3′), RIP3 siRNA (5′- CCAG CACUCUCGUAAUGAUTT -3′), and scrambled siRNA (5′-UUCUCCGAA CGUGUCACGUTT-3′) were all purchased from GenePharma Company (Suzhou, China). After siRNA transfection overnight, the cells were incubated with shikonin at indicated dosage for subsequent experiments.

### 2.8. Rat C6 tumor xenograft in mice

Twenty athymic BALB/c nude mice (aged 4 weeks, weight 20–22 g, Beijing Vital River laboratory animal technology company, China) were housed in a specific pathogen-free environment under the condition of 12-h light/12-h dark cycle, free access to food and water, and acclimatised to their surroundings for three days. The rats were cared in accordance with the guidelines for experimental animals of Jilin University and the study was approved by the ethics committee of the first hospital of Jilin University (Changchun, China). A total of $1 \times 10^7$ logarithmically growing C6 cells in 100 μL of PBS were subcutaneously injected into the right flank of each mouse. Therapeutic experiments were started when the tumor reached about 150 $mm^3$ after 7 days. The mice were allocated to receive intraperitoneal injections of vehicle (control group, n = 10/group), 2 mg/kg body weight shikonin in the same volume 50 μL once two days for four times (n = 10/group in each group). The tumor size was measured using a slide caliper, and the tumor volume was calculated using the formula: 0.5 × A × B2, in which A is the length of the tumor and B is the width. On the next day of the last treatment, the mice were euthanized by cervical dislocation. After being excised and weighed, the tumors were frozen immediately in liquid nitrogen for western blotting analysis.

### 2.9. Gel electrophoresis and western blotting

The collected glioma cells by centrifugation following harvest with a scraper and the frozen xenografted glioma tissue were homogenized with a glass Pyrex microhomogenizer (20 strokes) in ice cold Tris buffered saline (TBS; 15 mmol/L, pH 7.6) containing 250 mmol/L sucrose, 1 mmol/L magnesium chloride, 2.5 mmol/L EDTA, 1 mmol/L EGTA, 1 mmol/L dithiothreitol, 1.25 mg/mL pepstatin A, 10 mg/mL leupeptin, 2.5 mg/mL aprotinin, 1.0 mmol/L PMSF, 0.1 mmol/L sodium orthovanadate, 50 mmol/L sodium fluoride, and 2.0 mmol/L tetrasodium pyrophosphate. Homogenates were centrifuged at 1000 g for 10 min at 4 °C to obtain the supernatants. The protein content was determined using Bio-Rad protein assay kit. After SDS electrophoresis and transfer to PVDF membranes, the membranes were blocked with 3% bovine serum albumin in TBS for 30 min at room temperature, then incubated overnight at 4 °C with primary antibodies. After incubation with horseradish peroxidase-conjugated secondary antibody and the blots were washed, immunoreactive proteins were visualized on a chemi-luminescence developer (ChemiScope 5300, Clinx Science Instrument Company, Shanghai) and then the density was quantified by using software of Image J.

### 2.10. Co-immunoprecipitation

The collected SHG-44 glioma cells by centrifugation following harvesting with a scraper were homogenized as described above, and then centrifuged at 15,000 × *g* for 15 min at 4 °C to get the supernatant. The protein content was determined using Bio-Rad protein assay kit and protein concentrations were normalized. 400 μg protein samples were pre-cleared with isotype IgG control antibody (Abcam) and Protein A/G agarose (Millipore). 40 μL Protein A/G agarose prepared by incubation with 10 μL primary in 50 μL lysis buffer overnight at 4 °C was added into the protein samples, and then incubated overnight at 4 °C. Then the mixture was precipitated by high-speed freezing centrifugation at 12000 rpm for 10 s. To remove non-specifically bound proteins, the sediment was washed three times with lysis buffer. Agarose-bound immunocomplexes were then released by denaturing solution in loading buffer before performing a Western blot analysis.

### 2.11. Immunocytochemical staining

The cells seeded onto a culture dish in a diameter of 3 cm were fixed in ethanol, washed with PBS, and incubated with 1%Triton X-100 for 10 min. After the nonspecific antibody binding sites were blocked by 5% BSA (bovine serum albumin), the cells were incubated with primary antibody against *anti*-AIF antibody (1:100) or phospho-H2AX at serine 139 (1:100), respectively. Then, the cells incubated with in Cy3-conjugated goat anti-rabbit IgG (1:200) for 1 h at room temperature, followed by incubation with Heochst33258 for 30 min. Another group of SHG-44 cells were incubated with 100 nmol/L Mitotracker red for 30 min at 37 °C before fixation in ethanol. After the nonspecific antibody binding sites were blocked, the cells were incubated with *anti*-phospho-MLKL at S358 antibodies (1:100) followed by incubation in Cy3-conjugated goat anti-rabbit IgG (1:200) for 1 h and then with Heochst33258 for 30 min at room temperature. Finally, all the cells were visualized under laser scanning confocal microscope (Olympus FV1000, Tokyo, Japan).

### 2.12. Extraction of genomic DNA and agarose gel electrophoresis

The cells were harvested by using 0.25% trypsin and collected by centrifugation for 10 min at 2000 rev/min. Then, the collected cells were incubated overnight at 55 °C with constant shaking in 200 μL of SDS lysis buffer to extract the genomic DNA. A volume of each sample equivalent to 10 μg of DNA was mixed with 6 × DNA loading dye and subjected to gel electrophoresis on a 1% agarose gel. DNA bands on the gel were visualized by UV transillumination and gel images were captured on the Gel Doc instrument (Bio-Rad Laboratories, Hercules, CA).

### 2.13. Transmission electron microscopy

After the cells were harvested using 0.25% trypsin and then washed with PBS, they were collected by centrifugation for 10 min at 2000 revolutions per minute. Then, the cells were fixed in ice-cold 2.5% glutaraldehyde in PBS (pH 7.3), rinsed with PBS, post-fixed in 1% osmium tetroxide with 0.1% potassium ferricyanide, dehydrated through a graded series of ethanol (30%–90%) and embedded in Epon resin (Energy Beam Sciences, Agawam, MA, USA). Semithin (300 nm) sections were cut using a Reichart Ultracut ultra microtome, stained with 0.5% toluidine blue and examined under a light microscope. Ultrathin sections (65 nm) were stained with 1% uranyl acetate and 0.1% lead citrate and examined using a JEM2000EX transmission electron microscope (JEOL, Pleasanton, CA, USA).

### 2.14. Hoechst 33258 staining

The cells were seeded on coverslips in 6-well culture plates for 24 h, and then treated with shikonin for 2 h at 37 °C. After being washed twice with PBS, the cells were incubated with Hoechst 33258 dye (1 μg/mL) for 5 min at room temperature. After a final wash with PBS, the samples were visualized at 60 × magnification under a laser scanning confocal microscope (Olympus FV1000, Tokyo, Japan). The cells with chromatinolysis features were counted in five view fields which were selected randomly from each sample by a pathologist blind to this study, and presented as the percentage of total cells.

### 2.15. Statistical analysis

All data represent at least 4 independent experiments and are expressed as mean ± SD. Statistical comparisons were made using One-way ANOVA. P-values of less than 0.05 were considered to represent statistical significance.

## 3. Results

### 3.1. Shikonin induced chromatinolysis in glioma cells

In our previous study, we have found that shikonin significantly inhibited the viabilities of SHG-44, U251, U87 and C6 glioma cells in a concentration-dependent manner and the IC50 values of shikonin at 3 h were respectively 4 μmol/L in SHG-44 cells, 6 μmol/L in C6 cells, 10 μmol/L in U251 cells and U87 cells [17]. Thus, these dosages of shikonin were also used in this study.

Given that chromatinolysis is one of the final events leading to cell death [7], we investigated whether shikonin could induce chromatinolysis in glioma cells. To address this issue, transmission electron microscopy was used to examine shikonin-induced changes in chromatin. Compared with the smoothly outlined nucleus that contained clumps of heterochromatin (arrow heads) in control cells, the nucleus in the cells treated with shikonin for 3 h became electron-lucent despite the nuclear membrane was intact (Fig. 1A). This indicated that shikonin might induce chromatin degradation in glioma cells. Consistently, laser scanning confocal microcopy revealed that the nuclei detected by Hoechst 33258 which is a kind of blue fluorescence dyes and often used to stain nuclear DNA became hollowed in shikonin-treated cells when compared with the ones in control cells (Fig. 1B). Then, we analyzed the kinetics of shikonin-induced morphological changes in the nuclei of SHG-44 and U251 cells by counting the hollowed nuclei. It was found that the percentage of the hollowed nuclei to all the counted nuclei was improved significantly when shikonin treatment was extended from 1 h to 3 h (Fig. 1C). Considering that shikonin did not induce disruption in nuclear membrane and the volume of nucleus was in large volume, we

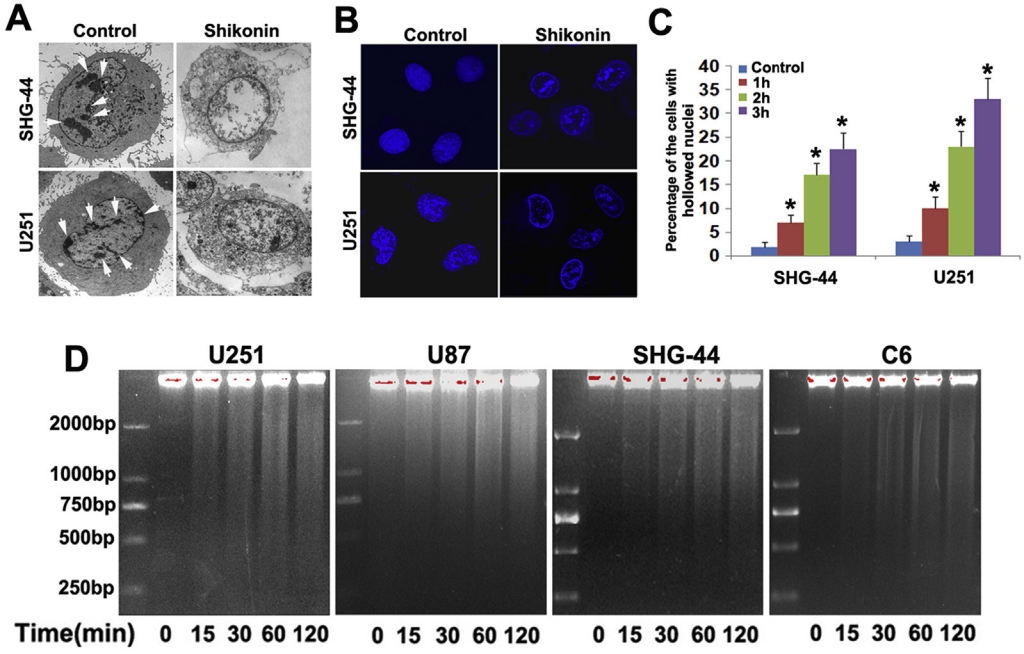


**Fig. 1. Shikonin induced chromatinolysis in glioma cells.**
(A)The representative images acquired by using transmission electronic microscope showed that nucleus in the SHG-44 and U251 glioma cell treated with shikonin at IC50 values for 3 h became electron-lucent with intact nuclear membrane, whereas the one in control group was outlined smoothly and contained clumps of heterochromatin (arrow heads). (B) Fluorescence microcopy combined with Hoechst 33258 staining revealed that the nuclei in the SHG44 and U251 glioma cells treated with shikonin at IC50 values for 3 h became hollowed when compared with those in control cells. (C) The formation of hollowed nuclei induced by shikonin were improved significantly when the incubation time was extended from 1 h to 3 h. (D)Agarose gel electrophoresis proved that the genomic DNA extracted from shikonin-treated U251, U87, SHG44 and C6 cells presented continuous smear bands, which became more apparent with the extension of treatment time from 15min to 120min. These results indicated that shikonin induced chromatinolysis in glioma cells. The values are expressed as mean ± SEM (n = 5 view fields). *: $p < 0.01$ versus control group.

thought that shikonin might induce DNA degradation (chromatinolysis) in glioma cells.

To demonstrate that shikonin could induce chromatinolysis in glioma cells, nuclear DNA was extracted from U251, U87, SHG-44 and C6 glioma cells which were treated with shikonin at the dosage of IC50 values for the indicated time and electrophoresed on agarose gel. Agarose gel electrophoresis is often used to separate DNA fragmentation induced by various stresses. In the condition of necrosis, DNA displayed smear bands on agarose gel [18]. Consistently, we found that the nuclear DNA extracted from the cells treated with shikonin presented continuous smear bands on agarose gel when compared with that in control group (Fig. 1D). Moreover, the smear bands became more apparent with the extension of shikonin treatment time from 15min to 120min. Thus, these data further verified that shikonin induced degradation of nuclear DNA.

### *3.2. MLKL contributed to shikonin-induced chromatinolysis and glioma cell necroptosis*

Accumulating evidences have demonstrated that shikonin induced glioma cell necroptosis via activation of RIP1 and RIP3 [11,17], in which the role of MLKL remains elusive. Thus, western blotting was used to analyze shikonin-induced changes in MLKL in U251, U87, SHG-44 and C6 glioma cells. As shown in Fig. 2A, when compared with those in control group, the protein levels of MLKL and phospho-MLKL (the active form of MLKL) were both obviously up-regulated in shikonin-treated cells, and their levels increased markedly when the incubation time was extended from 30min to 120min. This indicated that shikonin induced MLKL activation in a time-dependent manner.

To examine the role of MLKL activation in shikonin-induced glioma cell death, the cells were treated with MLKL inhibitor NSA at 10 μmol/L for 1 h and then incubated with shikonin at indicated concentrations for 3 h. As shown by LDH release assay, pretreatment with NSA significantly prevented the glioma cell death induced by shikonin at lower or higher dosages (Fig. 2B). Flow cytometry analysis combined with Annexin V-PI double staining is a usual method to differentiate necrotic cells from apoptotic ones. The cells at early stage of apoptosis are only positive to Annexin V, and the ones at late stage of apoptosis are positive to both Annexin V and PI. By contrast, the necrotic cells could be stained with either PI alone, or with Annexin V and PI [16]. Consistent with previous report [16], our data showed that shikonin induced time-dependent improvement in the cells positively stained with PI or both Annexin V and PI (Fig. 2C). This indicated that shikonin induced necrosis in glioma cells. However, pretreatment with NSA obviously decreased shikonin-induced glioma cell necrosis (Fig. 2D). Moreover, western blotting analysis revealed that shikonin-induced improvement in MLKL and phospho-MLKL were both prevented in the cell pretreated with NSA (Fig. 2E). Thus, these data suggested that MLKL regulated shikonin-induced glioma cell necrosis.

To further clarify the role of MLKL in shikonin-induced glioma cell death, small RNA interference (siRNA) was introduced to knock down of MLKL. When compared with the cells transfected with scrambled siRNA, shikonin-induced MLKL phosphorylation was mitigated when MLKL was knocked down with siRNA (Fig. 2F). Then, Flow cytometry analysis combined with Annexin V-PI double staining demonstrated that knockdown of MLKL with siRNA significantly prevented shikonin-induced glioma cell necrosis (Fig. 2G). This verified that MLKL contributed to shikonin-induced glioma cell necroptosis.

Notably, agarose gel electrophoresis of the nuclear DNA extracted from the cell treated with or without shikonin revealed that the smear bands of DNA induced by shikonin were alleviated obviously in the presence of MLKL inhibitor NSA or when MLKL was genetically knocked down with siRNA (Fig. 2H and I). Therefore, these data indicated that MLKL contributed to shikonin-induced glioma cell necroptosis via promotion of chromatinolysis.

### *3.3. MLKL promoted shikonin-induced γ-H2AX formation via improvement of ROS*

To clarify why MLKL could regulate chromatinolysis, we investigated its role in regulation of γ-H2AX (phospho-H2AX at ser139) formation that is a marker of DNA double strand breaks (DSBs) and regarded as a key step leading to chromatinolysis [10]. As shown by western blotting analysis, the level of γ-H2AX was improved markedly in the cells treated with shikonin for 3 h, which was reinforced with the increases of shikonin dosages (Fig. 3A). Moreover, many foci of γ-H2AX

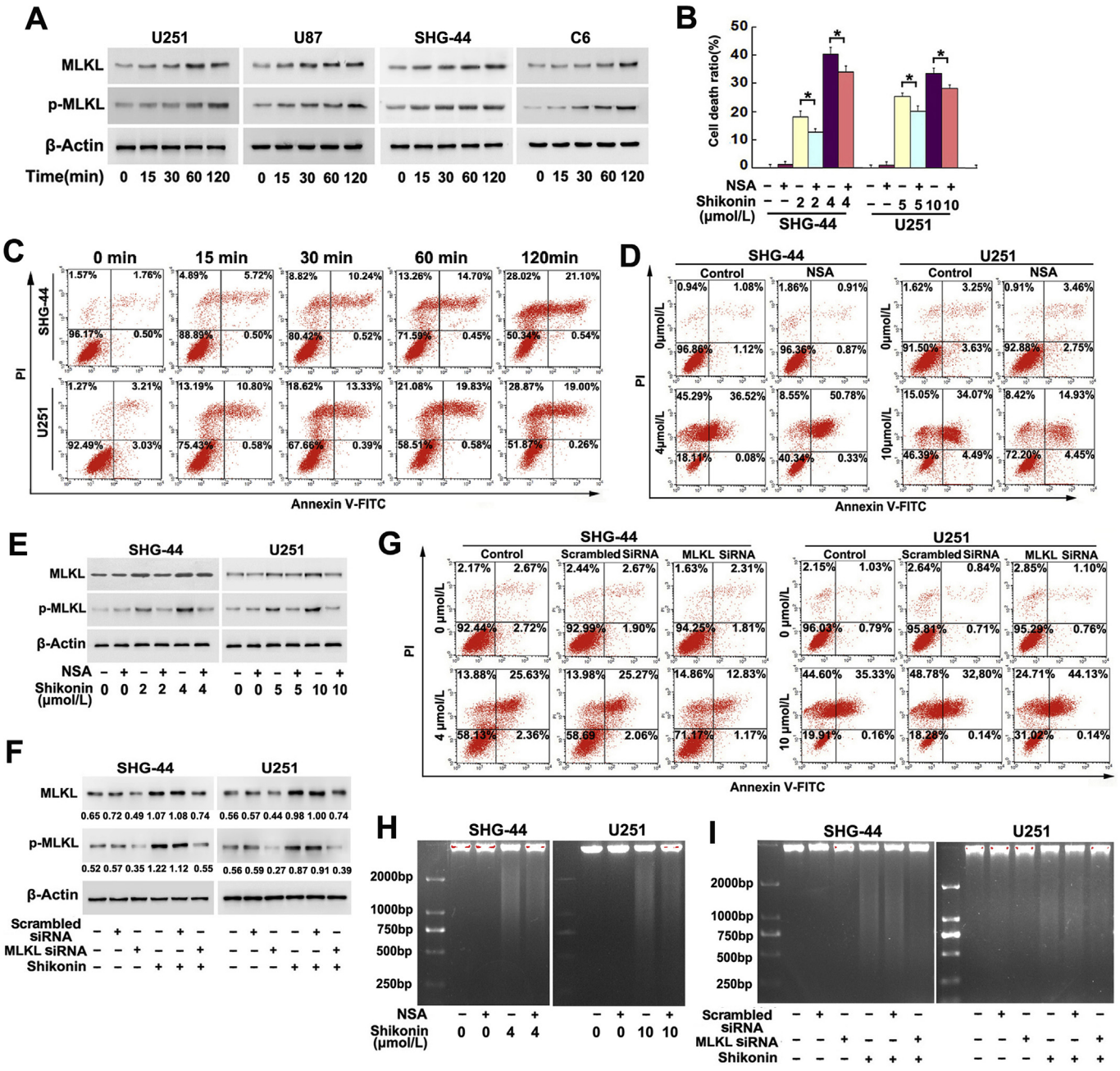


**Fig. 2. MLKL contributed to shikonin-induced glioma cell death.**
(A) Western blotting revealed that shikonin induced time-dependent upregulation of MLKL and phosphorylation of MLKL in U251, U87, SHG44 and C6 glioma cells. (B) LDH release assay demonstrated that pretreatment with MLKL specific inhibitor NSA prevented shikonin-induced glioma cell death. (C) Flow cytometry analysis combined with annexinV/PI double staining proved that shikonin induced time-dependent improvement in the cells that were positively stained with PI alone or with Annexin V and PI. (D) Flow cytometry analysis showed that shikonin-induced glioma cell necrosis was inhibited in the presence of NSA. (E) Western blotting analysis showed that NSA suppressed shikonin-induced improvement in the protein levels of MLKL and phospho-MLKL. (F) Knockdown of MLKL with siRNA prevented shikonin-induced expressional upregulation and phosphorylation of MLKL. (G)Flow cytometry analysis in combination with AnnexinV/PI double staining showed that knockdown of MLKL with siRNA prevented shikonin-induced glioma cell necrosis. (H) Agarose gel electrophoresis proved that pretreatment with NSA abrogated shikonin-induced chromatinolysis in SHG-44 and U251 glioma cells. (I) Agarose gel electrophoresis demonstrated as well that knockdown of MLKL with siRNA prevented shikonin-induced chromatinolysis in SHG-44 and U251 glioma cells. The values are expressed as mean ± SEM (n = 5 per group). *: $p < 0.01$.

(Red) were also observed in the nuclei (Blue) of shikonin-treated cells by using laser scanning confocal microscopy (Fig. 3B). Concomitantly, the phosphorylated levels of ataxia telangiectasia-mutated (ATM) and DNA-dependent protein kinase catalytic subunit (DNAPKcs) which are responsible for H2AX phosphorylation were both improved in shikonin-treated cells (Fig. 3A). By contrast, pretreatment with MLKL inhibitor NSA at 10 μmol/L for 1 h or knockdown of MLKL with siRNA significantly mitigated shikonin-induced upregulation of phospho-ATM, phospho-DNAPKcs and γ-H2AX (Fig. 3A and C). Therefore, these data indicated that MLKL promoted shikonin-induced γ-H2AX formation via causing phosphorylation of ATM or DNAPKcs.

Given that the activation of ATM and DNAPKcs are both secondary to DNA DSBs [10], we examined the role of MLKL in regulation of DNA DSBs by using neutral comet assay that is specifically designed to detect DNA DSBs. As shown in Fig. 3D, the cells treated with shikonin at IC50 values for 2 h had long comet tails when compared with the ones in

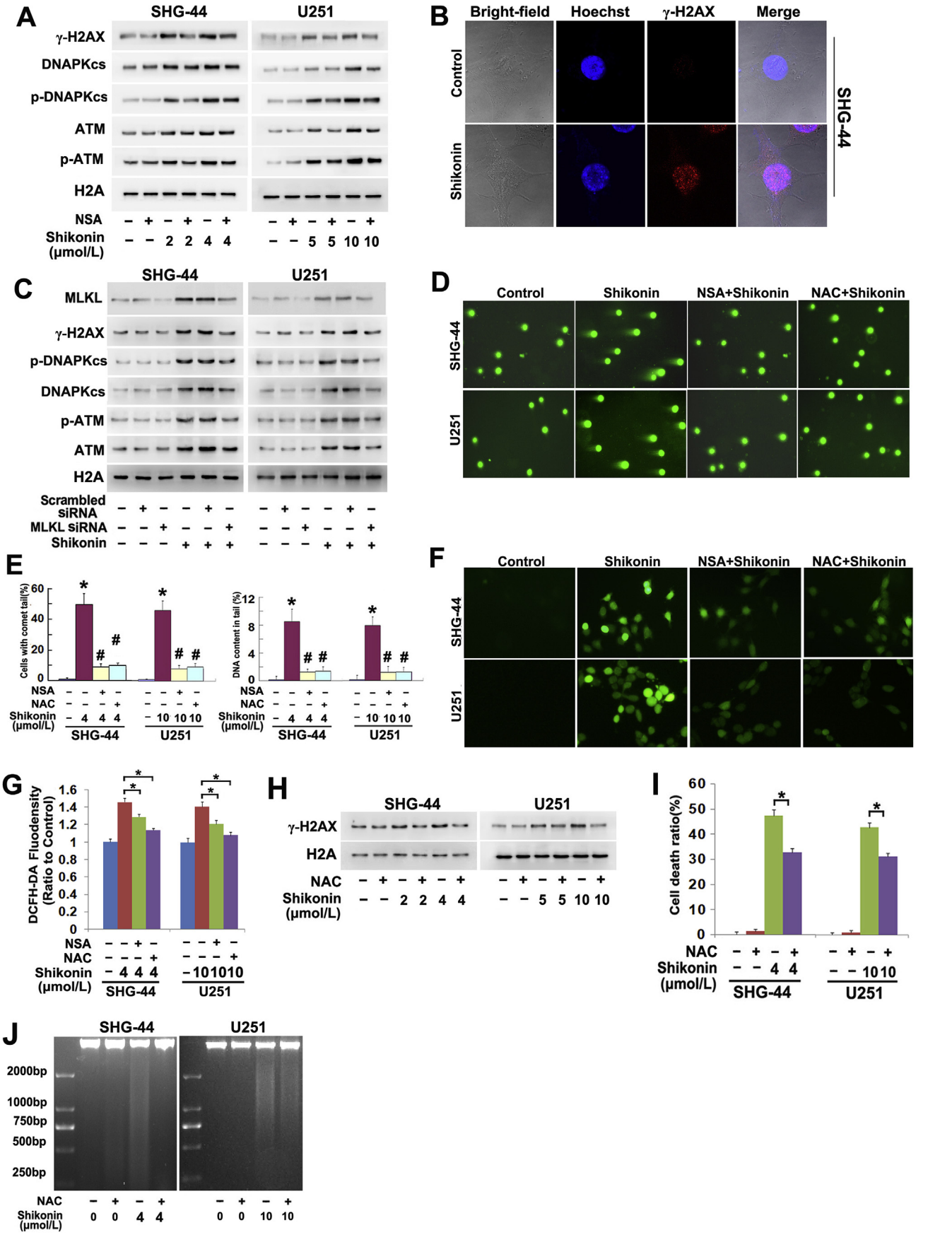


*(caption on next page)*

**Fig. 3. MLKL promoted shikonin-induced γ-H2AX formation via improvement of ROS.**
(A) Western blotting analysis showed that shikonin induced dosage-dependent improvement in γ-H2AX, phospho-ATM and phospho-DNAPKcs in SHG-44 and U251 glioma cells, which was prevented in the presence of MLKL inhibitor NSA. (B) Laser scanning confocal microscopy revealed that shikonin triggered formation of γ-H2AX (Red) in nucleus (Blue). (C) Knockdown of MLKL with siRNA prevented shikonin-induced phosphorylation of ATM and DNAPKcs and formation of γ-H2AX. (D) Neutral comet assay showed that majority of the SHG-44 and U251 cells treated with shikonin for 2 h had long comet tails, which were obviously inhibited when the cells were pretreated with MLKL inhibitor NSA or antioxidant NAC. (E) Statistical analysis demonstrated that pretreatment with NSA or NAC prevented shikonin-induced increases in the cells with comet tails and improvement of DNA content in the comet tails. (F) Representative images of the SHG-44 cells positively stained with ROS probe DCFH-DA under fluorescence microscope (20 ×). When compared with the control cells, the green fluorescence in the cells treated with shikonin at the dosage of IC50 values for 2 h was improved obviously, which was mitigated by pretreatment with NSA or NAC. (G) Statistical analysis of the fluorescence intensity detected by DCFH-DA demonstrated that NSA or NAC effectively suppressed shikonin-induced accumulation of intracellular ROS. (H) Western blotting analysis proved that shikonin-induced formation of γ-H2AX was prevented in the presence of NAC. (I) LDH release assay showed that shikonin-induced glioma cell death was inhibited in the presence of NAC. (J) Agarose gel electrophoresis revealed that pretreatment with NAC inhibited shikonin-induced chromatinolysis. The values are expressed as mean ± SEM (n = 5 per group). *: $p < 0.01$. (For interpretation of the references to color in this figure legend, the reader is referred to the Web version of this article.)

control group (Fig. 3D), which was also supported by the statistical analysis data showing that shikonin treatment not only obviously increased the cells with comet tails, but also improved the DNA content in the comet tails (Fig. 3E). However, the increases of the cells with comet tails and the improvement of DNA content in the comet tails induced by shikonin were both inhibited in the presence of NSA (Fig. 3D and E). This suggested that MLKL participated in regulation of shikonin-induced DNA DSBs in glioma cells.

Considering that ROS could lead to DNA DSBs [19], we examined the effect of activated MLKL on shikonin-induced overproduction of ROS. As revealed by fluorescence microscopy, when compared with that in control cells, the green fluorescence detected by ROS probe DCFH-DA became much brighter in the cells incubated with shikonin at the concentration of IC50 values for 2 h (Fig. 3F), which was also confirmed by the data from statistical analysis of the green fluorescence intensity (Fig. 3G). This suggested that shikonin induced improvement of intracellular ROS in glioma cells. By contrast, pretreatment with NSA 10 μmol/L for 1 h significantly prevented shikonin-induced increase in green fluorescence, indicating that MLKL promoted shikonin-induced overproduction of ROS (Fig. 3F and G).

To verify the role of ROS in shikonin-induced DNA DSBs, the cells were pretreated with antioxidant NAC at 5 mM for 1 h and then incubated with shikonin at IC50 values for 2 h. We found that NAC not only prevented shikonin-induced overproduction of ROS (Fig. 3F and G), but also suppressed shikonin-induced increases in the cells with comet tails, improvement of the DNA content in comet tail, γ-H2AX formation and glioma cell death (Fig. 3D, E, H and I). This indicated that ROS contributed to shikonin-induced DNA DSBs. Notably, agarose gel electrophoresis of the extracted nuclear DNA revealed that the smear band of DNA due to shikonin treatment was alleviated in the presence of NAC (Fig. 3 J).

Therefore, these results indicated that MLKL aggravated shikonin-induced chromatinolysis via promotion of ROS production.

### 3.4. MLKL aggravated shikonin-induced nuclear translocation of AIF

Because AIF translocation from mitochondria to nuclei contributed to both apoptotic and necrotic chromatinolysis [20], we examined whether shikonin could induce nuclear translocation of AIF. As shown by western blotting analysis, mitochondrial AIF was decreased obviously, but cytoplasmic and nuclear levels of AIF were both improved in the SHG-44 and U251 cells that were treated with shikonin for 2 h (Fig. 4A). This indicated that shikonin induced mitochondrial release of AIF and promoted AIF translocation into nucleus. Then, we found that both the decreases of mitochondrial AIF and the increases of nuclear AIF in SHG-44, U251, U87 and C6 cell became more apparent when shikonin treatment was extended from 15min to 120min (Fig. 4B). Moreover, laser scanning confocal microscopy showed as well that AIF accumulated in the nucleus of the cell treated with shikonin, when compared with that in control cell (Fig. 4C). This indicated that shikonin induced AIF release from mitochondrion and accumulation in nucleus.

To address the role of nuclear AIF in shikonin-treated glioma cells, we introduced siRNA to knock down AIF. Compared with the cells transfected with scrambled siRNA, shikonin-induced improvement of nuclear AIF was obviously inhibited when AIF was knocked down with siRNA (Fig. 4D). Moreover, LDH release assay showed that knockdown of AIF prevented shikonin-induced glioma cell death (Fig. 4E). Notably, agarose gel electrophoresis of the nuclear DNA demonstrated that the smear band of DNA resulting from shikonin treatment was markedly mitigated in the cells with knocked down AIF (Fig. 4F). This indicated that AIF contributed to shikonin-induced chromatinolysis and glioma cell death.

Then, we examined whether activated MLKL could regulate nuclear translocation of AIF by using western blotting analysis and found that inhibition of MLKL with NSA or knockdown of MLKL with siRNA could effectively inhibit shikonin-induced improvement in nuclear AIF (Fig. 4G and H). This indicated that activated MLKL aggravated shikonin-induced nuclear translocation of AIF.

### 3.5. Activated MLKL disturbed mitochondrial function

Given that mitochondrion is the normal location of AIF and AIF release from mitochondria is controlled by mitochondrial membrane potential [21], we examined whether shikonin treatment could result in mitochondria depolarization by using JC-1 staining. JC-1 presents high red fluorescence after accumulation in mitochondria, but exists in the cytoplasm when mitochondrial membrane potential depletes and emits green fluorescence. As shown in Fig. 5A and B, both fluorescence microscopy and flow cytometry analysis demonstrated that treatment with shikonin at the dosage of IC50 values for 2 h resulted in significant reduction of mitochondrial membrane potential. Considering that overproduced mitochondrial superoxide is a factor leading to mitochondrial membrane potential depletion, we examined shikonin-induced changes in the level of mitochondrial superoxide by using Mitosox red (a specific probe for mitochondrial superoxide). Fluorescence microscopy revealed that the red fluorescence detected by Mitosox red was much brighter in the cells treated with shikonin than that in the control cells (Fig. 5C). Statistical analysis of the red fluorescence density demonstrated as well that shikonin induced excessive generation of mitochondrial superoxide (Fig. 5D). By contrast, pretreatment with mitochondrial superoxide inhibitor MnTBAP at 40 μmol/L for 1 h could significantly prevent shikonin-induced mitochondrial generation of superoxide (Fig. 5C and D) and mitochondrial depolarization (Fig. 5A and B). Moreover, shikonin-induced abnormal increases of intracellular ROS, nuclear translocation of AIF and upregulation of γ-H2AX were all inhibited in the presence of MnTBAP (Fig. 5 E, F and G). This indicated the mitochondrial superoxide participated in regulation of shikonin-induced nuclear translocation of AIF and γ-H2AX formation.

Notably, pretreatment with NSA also prevented shikonin-induced mitochondrial generation of superoxide (Fig. 5C and D) and mitochondrial depolarization (Fig. 5A and B). Moreover, knockdown of

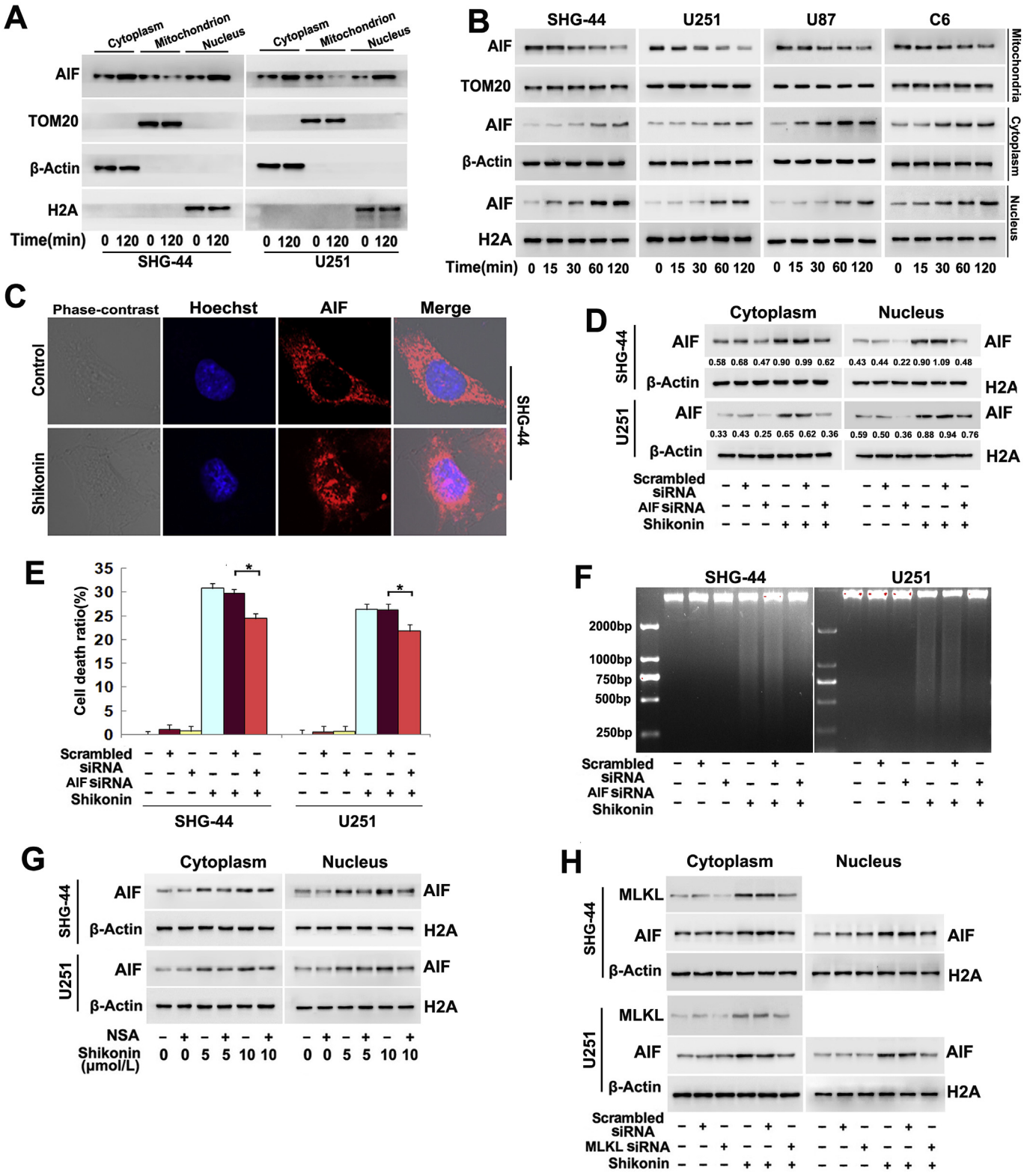


**Fig. 4. MLKL aggravated shikonin-induced nuclear translocation of AIF.**

(A) Western blotting analysis showed that treatment with shikonin at the dosage of IC50 values resulted in decrease of mitochondrial AIF, but increases of both cytoplasmic and nuclear AIF. (B)Shikonin induced time-dependent reduction of AIF in mitochondria, but improvement of AIF in cytoplasm and nucleus in SHG-44, U87, U251 and C6 glioma cell. (C) Representative images acquired with laser scanning confocal microscopy demonstrated that shikonin treatment resulted in accumulation of AIF (Red) in nucleus (Blue) of SHG-44 cell. (D) Knockdown of AIF with siRNA prevented shikonin-induced improvement in nuclear AIF. (E) LDH release assay proved that knockdown of AIF prevented shikonin-induced death in SHG-44 and U251 glioma cells. (F) Agarose gel electrophoresis proved that knockdown of AIF inhibited shikonin-induced chromatinolysis in SHG-44 and U251 cells. (G and H) Shikonin-induced improvement of nuclear AIF levels were inhibited in the presence of MLKL inhibitor NSA or when MLKL was knocked down with siRNA. The values are expressed as mean ± SEM (n = 5 per group). *: $p < 0.01$. (For interpretation of the references to color in this figure legend, the reader is referred to the Web version of this article.)

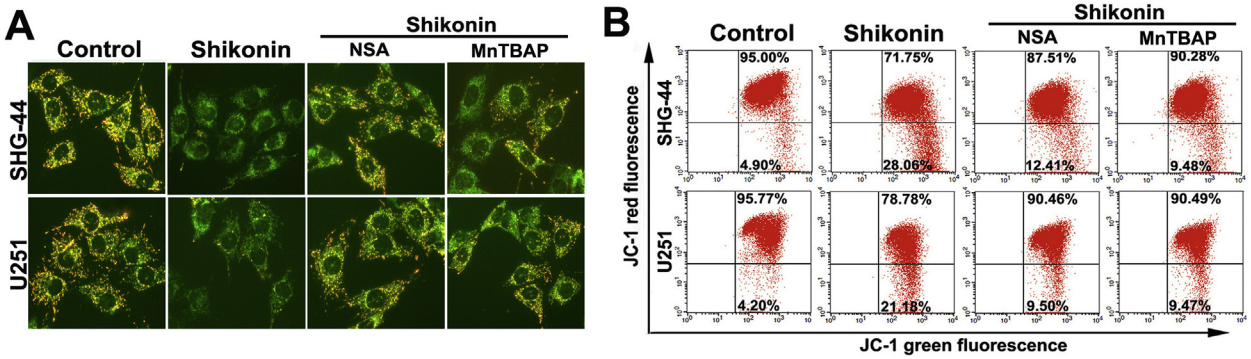


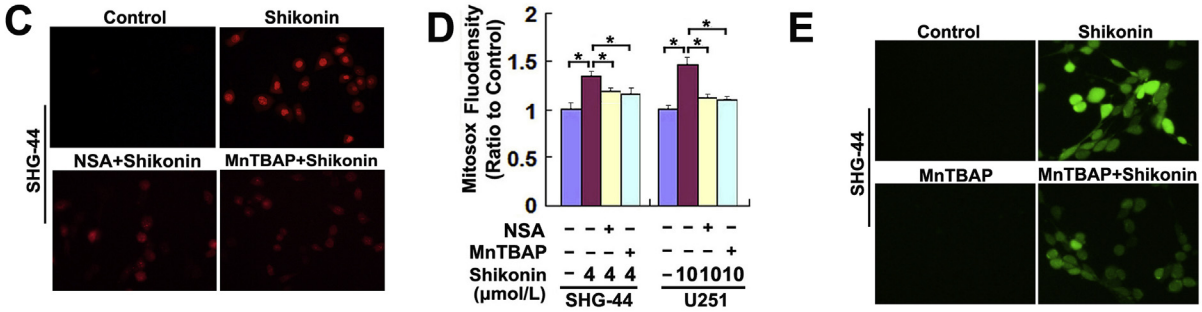


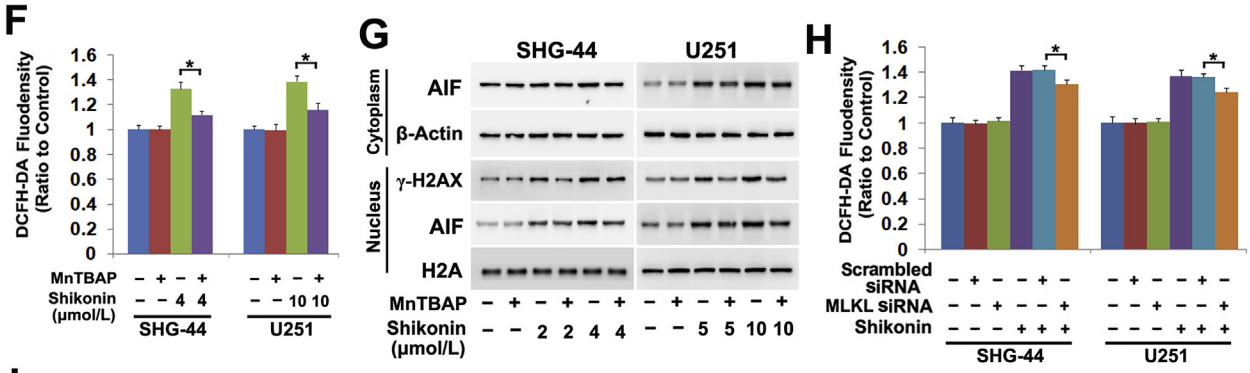


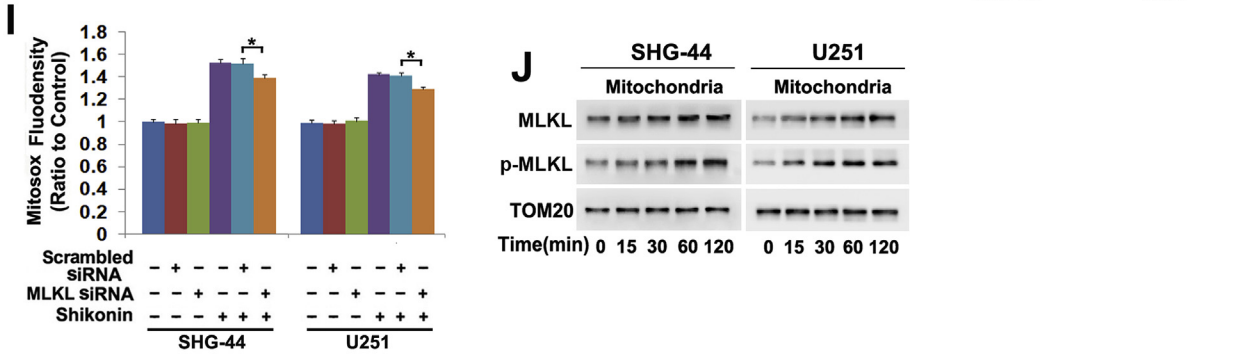


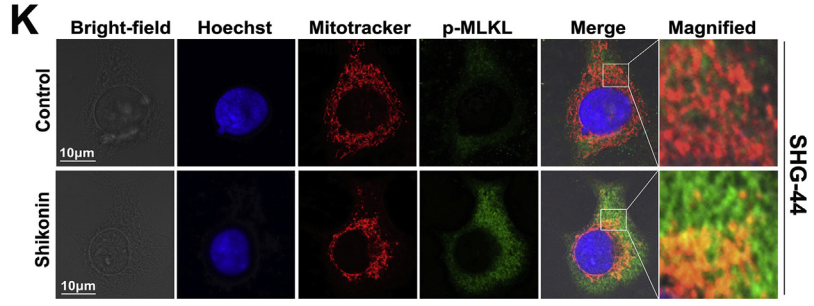


(caption on next page)

**Fig. 5. MLKL activation resulted in mitochondria damage.**
(A) Fluorescence microscopy combined with JC-1 staining revealed that the red fluorescence decreased obviously in the SHG-44 and U251 cells treated with shikonin at the dosages of IC50 values for 1 h, which was reversed in the presence of MLKL inhibitor NSA or mitochondrial superoxide inhibitor MnTBAP. (B) Flow cytometry analysis with JC-1 staining showed as well that shikonin-induced depletion of mitochondrial membrane potential was obviously inhibited in the presence of NSA or MnTBAP. (C) Representative images of the SHG-44 glioma cells incubated with mitochondrial superoxide probe Mitosox red under fluorescence microscope (20 × ). Shikonin treatment resulted in significant improvement in the red fluorescence, which was mitigated in the presence of MLKL inhibitor NSA or mitochondrial superoxide inhibitor MnTBAP. (D) Statistical analysis of the intensity of the red fluorescence detected by Mitosox red revealed that pretreatment with NSA or MnTBAP suppressed the generation of mitochondrial superoxide induced by shikonin. (E) Representative images of the SHG-44 cells stained with ROS probe DCFH-DA under fluorescence microscope showed that shikonin-induced improvement in the green fluorescence was markedly inhibited in the presence of MnTBAP (20 × ). (F) Statistical analysis of the fluorescence intensity demonstrated that MnTBAP effectively suppressed shikonin-induced accumulation of intracellular ROS. (G) Western blotting analysis revealed that shikonin-induced nuclear translocation of AIF was inhibited when the cells were pretreated with MnTBAP. (H) Knockdown of MLKL with siRNA mitigated shikonin-induced improvement of intracellular ROS. (I) The overproduced mitochondrial superoxide caused by shikonin was prevented when MLKL was knocked down with siRNA. (J) Western blotting showed that shikonin treatment induced obvious improvement of MLKL and phospho-MLKL in mitochondria. (K) The representative confocal images showed that phospho-MLKL (green) localized at mitochondria (red) in the SHG-44 cells treated with shikonin at the dosage of IC50 value for 2 h. The values are expressed as mean ± SEM (n = 5 per group). *: $p < 0.01$. (For interpretation of the references to color in this figure legend, the reader is referred to the Web version of this article.)

MLKL with siRNA not only prevented shikonin-induced improvement of intracellular ROS, but also mitigated the abnormal increase of mitochondrial superoxide caused by shikonin (Fig. 5H and I). Thus, we isolated mitochondria by using differential centrifuge and examined the protein levels of MLKL and its active form phospho-MLKL in mitochondria by using western blotting analysis. As shown in Fig. 5J, when compared with those in control cells, mitochondrial levels of MLKL and phospho-MLKL were both improved by shikonin in a time-dependent manner. Consistently, laser scanning confocal microscopy revealed that shikonin induced accumulation of phospho-MLKL (green) on mitochondria (Red) (Fig. 5K). This indicated that activated MLKL disturbed mitochondrial function, which resulted in excessive generation of mitochondrial superoxide.

### 3.6. Shikonin induced MLKL activation and chromatinolysis in glioma cells in vivo

To test whether shikonin could induce MLKL activation and chromatinolysis in vivo, C6 glioma cells were xenografted subcutaneously into the flank of nude mice as reported previously [17]. After being treated with shikonin at the dosage of 2 mg/kg once two days, the volume of the xenografted glioma was obviously smaller than that in control group at day 8 (Fig. 6A). Statistical analysis of the tumor volume proved as well that shikonin treatment significantly inhibited the growth of xenografted glioma (Fig. 6B). Then, we sacrificed the mice and conducted agarose gel electrophoresis of the extracted nuclear DNA from the removed gliomas. It was found the genomic DNA extracted from shikonin-treated gliomas also presented smear band on agarose gel (Fig. 6C), indicating that shikonin-induced chromatinolysis in vivo. Furthermore, we isolated cytoplasm, nucleus and mitochondrion fractions by using differential centrifuge and analyzed the levels of target proteins in different fractions. As shown by western blotting analysis, phospho-MLKL was induced to up-regulate by shikonin not only in cytoplasm, but also in mitochondria (Fig. 6D). This indicated that shikonin induced MLKL activation and activated MLKL accumulated at mitochondria. We also found that shikonin treatment resulted in decreases in mitochondrial AIF, but improved cytoplasmic and nuclear levels of AIF (Fig. 6E and F). Moreover, nuclear levels of γ-H2AX, phospho-ATM and phospho-DNAPKcs were all up-regulated in shikonin-treated gliomas (Fig. 6G). Therefore, these indicated that shikonin induced nuclear translocation of AIF and γ-H2AX formation in glioma cells in vivo.

### 3.7. Shikonin induced a positive feedback between MLKL and its upstream signals

Given that shikonin could induce activation of RIP3 and activated RIP3 accounts for MLKL phosphorylation during the process of necroptosis [1,17], the cells were respectively transfected with scrambled siRNA and RIP3 siRNA and then incubated with shikonin at the dosage of IC50 values for 3 h. As revealed by western blotting analysis, knockdown of RIP3 with siRNA not only prevented shikonin-induced phosphorylation of RIP3, but also mitigated the phosphorylated level of MLKL (Fig. 7A). Then, co-immunoprecipitation was used to test whether MLKL was recruited to RIP3 in the presence of shikonin. As shown in Fig. 7B, when RIP3 was immunoprecipitated with its antibody, MLKL was co-immunoprecipitated as well. Moreover, the levels of RIP3 and co-immunoprecipitated MLKL were both improved when the dosage of shikonin was increased from 2 μmol/L to 4 μmol/L. Thus, these indicated that RIP3 regulated shikonin-induced activation of MLKL.

Then, we tested whether activated MLKL could reversely regulate its upstream signal RIP3. As revealed by western blotting analysis, shikonin-induced expressional upregulation of RIP3 and phospho-RIP3 (the active form of RIP3) were both inhibited in the SHG-44 and U251 cells pretreated with MLKL inhibitor NSA at 10 μmol/L for 1 h (Fig. 7C). Similar results could be found when MLKL was knocked down with siRNA (Fig. 7D). To clarify why MLKL could reversely regulate the activation of RIP3, we examined the protein levels of phospho-RIP1 (the active form of RIP1) and CYLD, because RIP3 could be activated by RIP1 and CYLD could promote RIP1 activation via deubiquitinating it [22,23]. We found that the up-regulated levels of RIP1, phospho-RIP1 and CYLD induced by shikonin were all prevented in the presence of NSA or when MLKL was knocked down with siRNA (Fig. 7C and D). This indicated that activated MLKL could reversely promote the activation of RIP1. Given that ROS could promote the activation of RIP1 and RIP3 [11], the SHG-44 and U251 cells were pretreated with antioxidant NAC at 5 mmol/L for 1 h and then incubated with shikonin at the dosage of IC50 values for 3 h. As revealed by western blotting analysis, we found that shikonin-induced improvement in the protein levels of CYLD, phospho-RIP1 and phospho-RIP3 were all prevented in the presence of NAC (Fig. 7E). Moreover, co-immunoprecipitation analysis proved that the interaction between RIP3 and MLKL induced by shikonin was inhibited in the cells pretreated with NAC (Fig. 7F). This indicated that ROS reinforced shikonin-induced activation of RIP1 and RIP3. Considering that MLKL could promote shikonin-induced accumulation of intracellular ROS, we thought that MLKL reversely regulate the activation of its upstream signals RIP1 and RIP3 via improvement of ROS generation.

## 4. Discussion

In summary, we found in this study that shikonin induced MLKL activation and chromatinolysis in glioma cells in vitro and in vivo, which were accompanied with nuclear translocation of AIF and γ-H2AX formation. In vitro studies revealed that inhibition of MLKL with its specific inhibitor NSA or knockdown of MLKL with siRNA abrogated shikonin-induced glioma cell death, as well as chromatinolysis. Mechanistically, activated MLKL targeted mitochondria and triggered

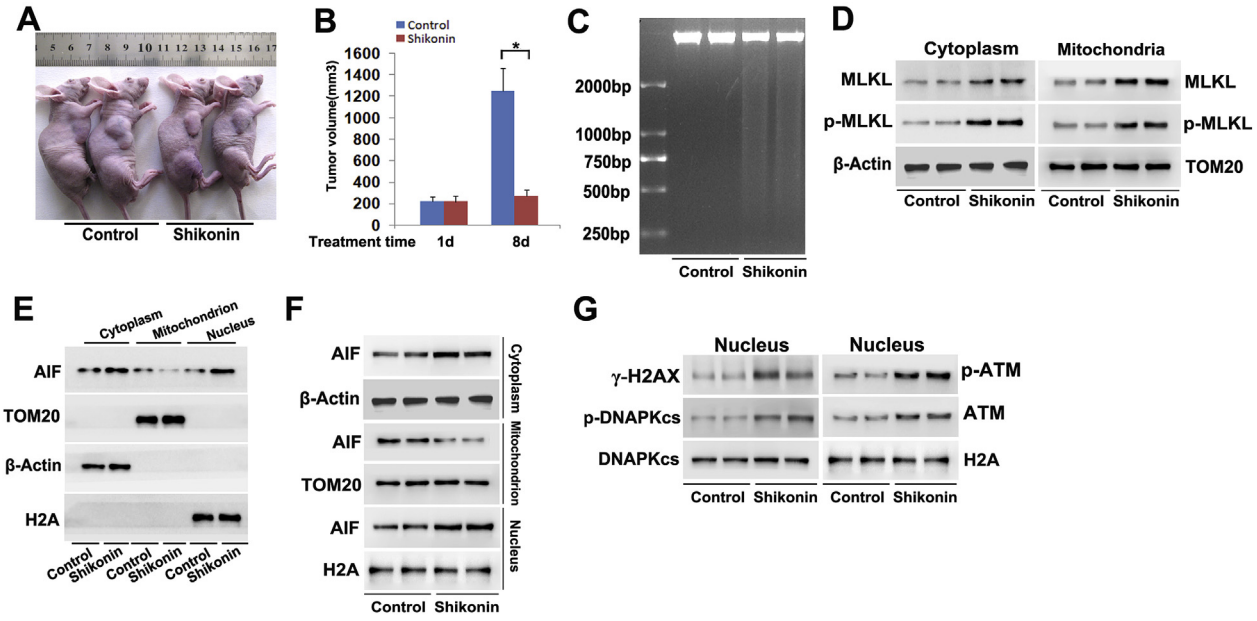


**Fig. 6. Shikonin induced MLKL activation and chromatinolysis in glioma cells in vivo.**
(A)Representative images of the mice with xenografted glioma. (B) Shikonin treatment inhibited the growth of xenografted glioma. (C)Agarose gel electrophoresis of the extracted nuclear DNA from the gliomas treated with or without shikonin showed that shikonin induced chromatinolysis in vivo. (D) Western blotting analysis showed that shikonin induced obvious upregulation of MLKL and phospho-MLKL in mitochondria. (E and F) Shikonin improved both cytoplasmic and nuclear levels of AIF, but decreased mitochondrial AIF level. (G) Shikonin induced γ-H2AX formation and activation of ATM and DNAPKcs. The values are expressed as mean ± SEM (n = 10 per group). *: $p < 0.01$.

excessive generation of mitochondrial superoxide, which promoted AIF translocation into nucleus via causing mitochondrial depolarization and γ-H2AX formation through improving intracellular accumulation of ROS. By contrast, inhibition of nuclear level of AIF by knocking down of AIF with SiRNA or mitigation of γ-H2AX formation by suppressing ROS with antioxidant NAC effectively prevented shikonin-induced chromatinolysis. Then, we found that RIP3 interacted with and activated MLKL during the process of shikonin-induced glioma cell necroptosis. Notably, activated MLKL was found to reversely up-regulate the protein level of CYLD and promote the activation of RIP1 and RIP3 via improvement of intracellular ROS levels. Taken together, our data suggested that MLKL contributed to shikonin-induced glioma cell necroptosis via regulation of chromatinolysis, and shikonin induced a positive feedback between MLKL and its upstream signals RIP1 and RIP3 (Fig. 8).

Chromatinolysis was found to be involved in apoptosis and necrosis [24,25]. It was found that DNA was cleaved into fragments of approximate 180-200bp by activated endonucleases such as caspase-activated DNase (CAD) and endonuclease G in the cells stressed with apoptosis inducers [7]. However, chromatinolysis in necrotic cells was rapid and DNA was cleaved randomly [25]. This explained why the nuclear DNA extracted from apoptotic cells presented ladder bands after being electrophoresed on agarose gel, whereas the DNA extracted from necrotic cells displayed continuous smear pattern [25]. In this study, clumps of chromatin (a complex of DNA and histone protein) which appeared in control cells could not be observed in shikonin-treated cells under transmission electronic microscope. Moreover, shikonin induced time-dependent enhancement of smear DNA bands on agarose gel. By contrast, the random cleavage of DNA and the glioma cell death induced by shikonin were both prevented in the presence of MLK inhibitor NSA or when MLKL was genetically knocked down with siRNA. This suggested that MLKL contributed to shikonin-induced glioma cell death via promotion of chromatinolysis.

Although the mechanism responsible for necrotic chromatinolysis remains elusive, several endonucleases such as DNase1 and DNaseγ were reported to regulate necrotic chromatinolysis [26,27]. However, nuclear translocation of AIF and γH2AX formation was respectively demonstrated to play important roles in promotion of chromatinolysis during the process of necroptosis [10]. As a flavoprotein normally contained in mitochondrial inter-membrane space, AIF functioned as an endonuclease to degrade DNA after being truncated and redistribution into nucleus [28]. Within nucleus, AIF was recruited by γH2AX and then cooperated with cyclophilin A to form a DNA-degrading complex [10,28]. It was also reported that AIF was also required for nuclear recruitment of macrophage migration inhibitory factor (MIF), which is a newly-found nuclease that could cleave genomic DNA into large fragments [29]. Thus, AIF played an important role in regulation of chromatinolysis. In this study, we found that shikonin induced time-dependent nuclear translocation of AIF and γH2AX formation. Although AIF cleaves DNA in large scale (approximate 50kbp) in the condition of apoptosis, it was also proven to cleaving DNA randomly when ATP generation was inhibited [19]. Our previous report showed that shikonin which could inhibit PKM2 and induced significant decrease of ATP via causing glycolysis dysfunction in glioma cells [30,31]. This might explain why the DNA extracted from shikonin-treated cells displayed smear band on agarose gel after electrophoresis. Particularly, we found in this study that shikonin-induced random cleavage of DNA was prevented when AIF was knocked down with siRNA, indicating that AIF contributed to shikonin-induced chromatinolysis.

Accumulating evidences demonstrated that oxidative stress characterized with intracellular accumulation of ROS could promote chromatinolysis, given that ROS could lead to both γH2AX formation and nuclear translocation of AIF. It was found that improvement of mitochondrial superoxide generation by using rotenone (an inhibitor of mitochondrial respiratory chain) resulted in mitochondrial depolarization in PC12 cells [32,33]. Moreover, in the glioma cells that were stressed with hydrogen peroxide which is a member of ROS, AIF was found to translocate from mitochondria into nucleus [34]. Previous report showed that shikonin treatment could lead to time-dependent overproduction of ROS in glioma cells [17]. In this study, we found shikonin induced abnormal generation of mitochondrial superoxide, whereas suppression of mitochondrial superoxide with MnTBAP

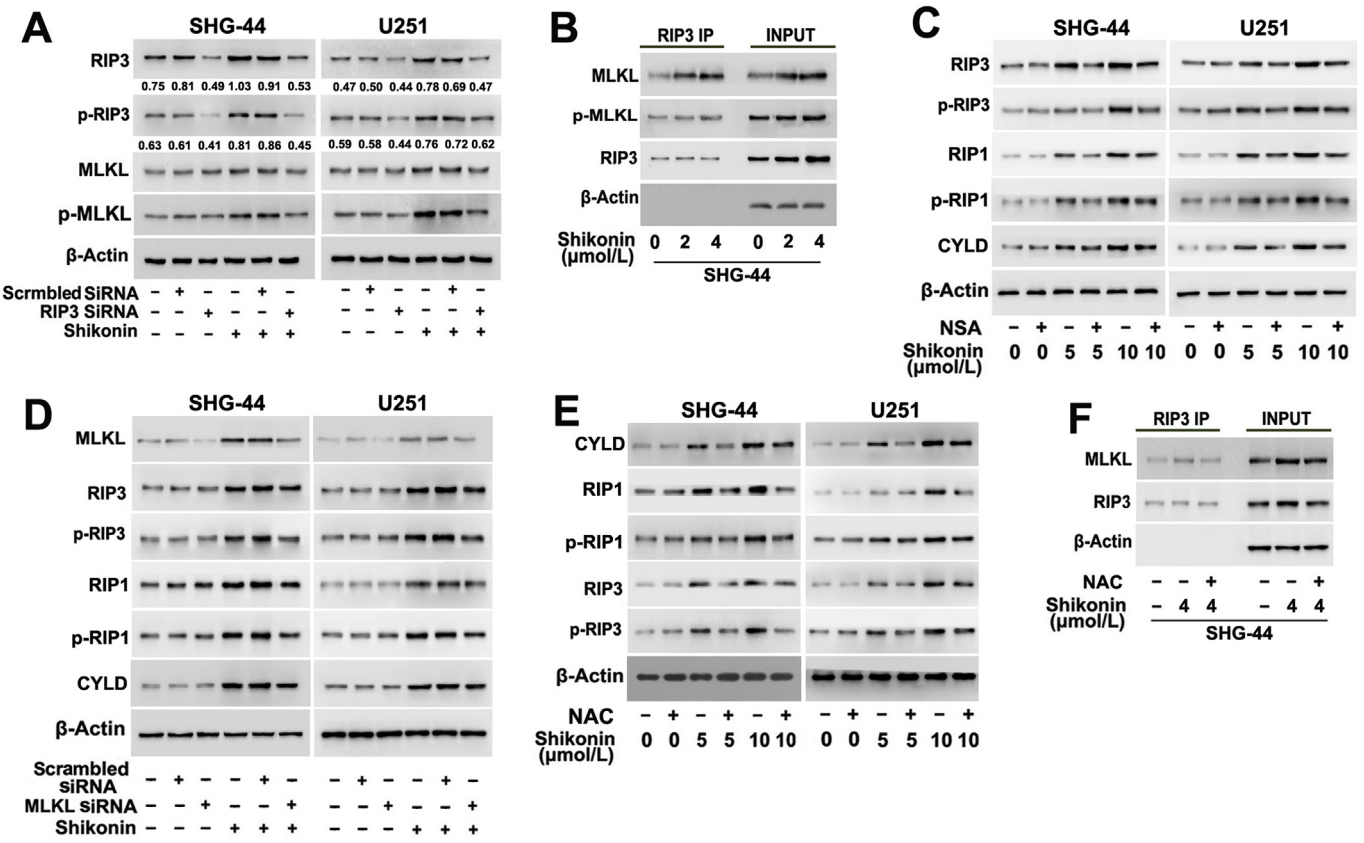


**Fig. 7. RIP3 contributed to shikonin-induced MLKL activation and MLKL reversely promoted the phosphorylation of RIP1 and RIP3.**
(A) Western blotting analysis showed that knockdown of MLKL with siRNA prevented shikonin-induced phosphorylation of RIP3 and MLKL. (B) Co-immunoprecipitation revealed that MLKL was co-immunoprecipitated when RIP3 was immunoprecipitated with its antibody. Moreover, the levels of co-immunoprecipitated MLKL and phospho-MLKL were both improved with the increase of shikonin dosage from 2 μmol/L to 4 μmol/L. (C) Western blotting analysis proved that shikonin-induced improvement in the protein levels of RIP1, phospho-RIP1, RIP3, phospho-RIP3 and CYLD were suppressed in the presence of MLKL inhibitor NSA. (D) Knockdown of MLKL with siRNA prevented shikonin-induced expressional upregulation of RIP1, RIP3 and CYLD, and phosphorylation of RIP1 and RIP3. (E) The improved level of CYLD, RIP1 and RIP3 and the increased phosphorylation of RIP1 and RIP3 resulting from shikonin treatment were all prevented in the presence of NAC. (F) Co-immunoprecipitation analysis showed that NAC inhibited shikonin-induced interaction between RIP3 and MLKL. These indicated that MLKL reversely regulate the activation of its upstream signals RIP1 and RIP3 via improvement of ROS generation.

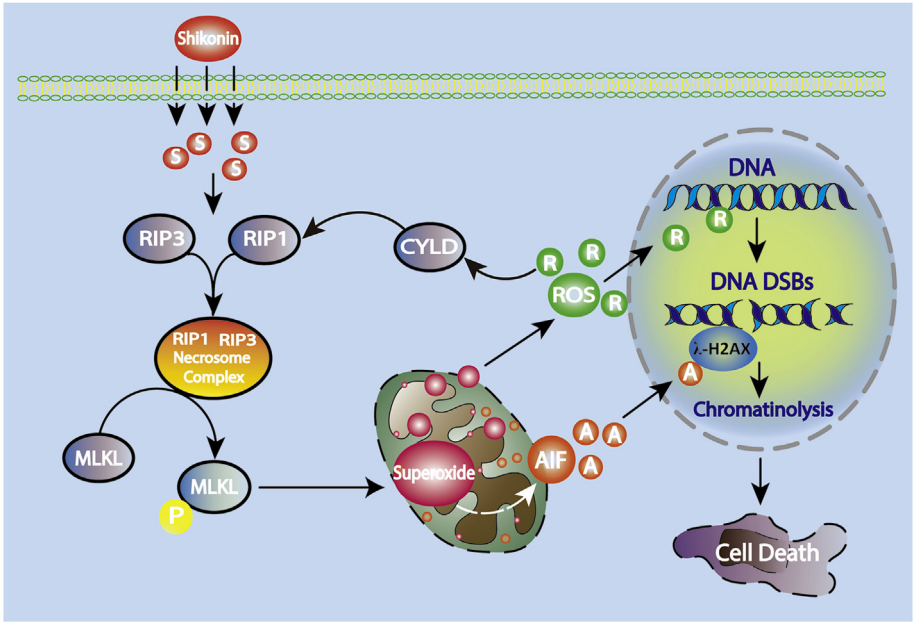


**Fig. 8.** Schematic model for the role of MLKL in shikonin-induced necroptosis and chromatinolysis.

inhibited mitochondrial depolarization and nuclear accumulation of AIF. Additionally, ROS could attack DNA to produce DNA DSBs, which resulted in activation of ATM and DNAPKcs, and then γH2AX formation [35]. It was found in this study that shikonin induced DNA DSBs, formation of γH2AX and activation of ATM and DNAPKcs, which were all abrogated when intracellular ROS levels were suppressed by antioxidant NAC. Notably, agarose gel electrophoresis proved that shikonin-induced chromatinolysis was also inhibited in the presence of NAC. Briefly, oxidative stress contributed to shikonin-induced chromatinolysis.

Shikonin could improve intracellular ROS in glioma cells via multiple pathways such as activation of NADPH oxidase and lipoxygenases [36]. In this study, we found that activated MLKL aggravated shikonin-induced oxidative stress given that inhibition of activated MLKL with NSA obviously mitigated shikonin-induced accumulation of intracellular ROS. Consistently, previous studies showed as well that activated MLKL was involved in improving intracellular ROS levels. Zhao et al. reported that MLKL was required for ROS production during the process of TNF-induced necrosis in colorectal carcinoma HT-29 cells [37]. Schenk et al. proved that knockdown of MLKL decreased BV6/TNFα-induced ROS generation in human FADD-deficient Jurkat cells [38]. Although how MLKL regulates ROS generation is still elusive, it was reported that activated MLKL could bind with mitochondrial cardiolipin, which is an important component of mitochondrial inner membrane and supports assembly and interaction of mitochondrial respiratory chain complexes and supercomplexes [39,40]. In this study, we found that the activated MLKL induced by shikonin relocated on mitochondria. Inhibition of MLKL with NSA suppressed obviously shikonin-induced excessive generation of mitochondrial superoxide, and mitigation of mitochondrial superoxide with MnTBAP prevented the increases of intracellular ROS. Thus, activated MLKL might promote shikonin-induced generation of ROS via disturbing mitochondrial respiratory chain in glioma cells.

The activation of MLKL is mainly regulated by its upstream signal RIP3 after it was recruited into the necrosome complex consisting of RIP1 and RIP3 [41]. In this study, we found that MLKL was bound to RIP3 by using co-immunoprecipitation, and knockdown of RIP3 with siRNA significantly suppressed shikonin-induced MLKL phosphorylation. Previously, it was reported that shikonin induced necroptosis in glioma, osteosarcoma and pancreatic cancer via activation of RIP1 and RIP3 [17,42,43]. In this study, we demonstrated that MLKL was a downstream signal of RIP1 and RIP3 in shikonin-induced glioma cell necroptosis. Notably, we found in this study that inhibition of MLKL activation with NSA or knockdown of MLKL with siRNA obviously attenuated shikonin-induced phosphorylation of both RIP1 and RIP3 and expressional upregulation of CYLD. Similarly, knockdown of MLKL with siRNA was reported to inhibit necrosome assembly in the cortical neurons stressed by oxygen glucose deprivation plus caspase inhibitor z-VAD treatment [44]. Thus, these suggested that MLKL could reversely regulate shikonin-induced activation of RIP1 and RIP3 in glioma cells.

Although it remains unclear about the factors accounting for the regulatory effect of MLKL on the activation of RIP1 and RIP3, recent studies demonstrated that ROS could regulate the process of necroptosis. Zhao et al. reported that hydrogen peroxide induced necroptosis in rat nucleus pulposus cells through activation of RIP1 and RIP3 pathway [45]. Huang et al. found that ROS enhanced the interaction between RIP1 and RIP3 in colorectal cancer cells challenged by hypoxia [46]. Therefore, ROS played an important role in promotion of necrosome complex formation and activation of RIP1 and RIP3. In this study, we found that mitigation of ROS with antioxidant NAC markedly prevented shikonin-induced phosphorylation of RIP1 and RIP3 and expressional upregulation of CYLD. Considering that activated MLKL could increase the levels of intracellular ROS, we thought that activated MLKL reversely enhance shikonin-induced activation of RIP1 and RIP3 and expressional upregulation of CYLD via improvement of intracellular ROS. Therefore, we thought that shikonin induced a positive feedback between MLKL and its upstream signals RIP1 and RIP3 in glioma cells.

In conclusion, we demonstrate that in this study that shikonin induces activation of MLKL in a time-dependent manner, and activated MLKL contributes to glioma cell necroptosis via triggering of chromatinolysis by promotion of nuclear translocation of AIF and γ-H2AX formation. Moreover, MLKL enhances shikonin-induced activation of its upstream signals RIP1 and RIP3 via improvement of intracellular ROS by disturbing mitochondrial function.

## Declaration of competing interest

The authors declare that they have no conflict of interests.

## Acknowledgments

This work was supported by National Nature and Science Foundation of China (81372697, 81772669, and 81772657), Changbaishan Scholar Project of Jilin province (2013026), and Scientific Research Foundation of Jilin province (20190701051GH).

## References

[1] L. Sun, H. Wang, Z. Wang, S. He, S. Chen, D. Liao, L. Wang, J. Yan, W. Liu, X. Lei, X. Wang, Mixed lineage kinase domain-like protein mediates necrosis signaling downstream of RIP3 kinase, Cell 148 (2012) 213–227.
[2] Z. Cai, S. Jitkaew, J. Zhao, H.C. Chiang, S. Choksi, J. Liu, Y. Ward, L.G. Wu, Z.G. Liu, Plasma membrane translocation of trimerized MLKL protein is required for TNF-induced necroptosis, Nat. Cell Biol. 16 (2014) 55–65.
[3] X. Chen, W. Li, J. Ren, D. Huang, W.T. He, Y. Song, C. Yang, W. Li, X. Zheng, P. Chen, J. Han, Translocation of mixed lineage kinase domain-like protein to plasma membrane leads to necrotic cell death, Cell Res. 24 (2014) 105–121.
[4] H. Wang, L. Sun, L. Su, J. Rizo, L. Liu, L.F. Wang, F.S. Wang, X. Wang, Mixed lineage kinase domain-like protein MLKL causes necrotic membrane disruption upon phosphorylation by RIP3, Mol. Cell 54 (2014) 133–146.
[5] B. Xia, S. Fang, X. Chen, H. Hu, P. Chen, H. Wang, Z. Gao, MLKL forms cation channels, Cell Res. 26 (2016) 517–528.
[6] S.A. Conos, K.W. Chen, D. De Nardo, H. Hara, L. Whitehead, G. Núñez, S.L. Masters, J.M. Murphy, K. Schroder, D.L. Vaux, K.E. Lawlor, L.M. Lindqvist, J.E. Vince, Active MLKL triggers the NLRP3 inflammasome in a cell-intrinsic manner, Proc. Natl. Acad. Sci. U.S.A. 114 (2017) E961–E969.
[7] K. Kawane, K. Motani, S. Nagata, DNA degradation and its defects, Cold Spring Harb. Perspect. Biol. 6 (2014), https://doi.org/10.1101/cshperspect.a016394.
[8] C. Artus, H. Boujrad, A. Bouharrour, M.N. Brunelle, S. Hoos, V.J. Yuste, P. Lenormand, J.C. Rousselle, A. Namane, P. England, H.K. Lorenzo, S.A. Susin, AIF promotes chromatinolysis and caspase-independent programmed necrosis by interacting with histone H2AX, EMBO J. 29 (2010) 1585–1599.
[9] S. Nagata, DNA degradation in development and programmed cell death, Annu. Rev. Immunol. 23 (2005) 853–875.
[10] M. Baritaud, L. Cabon, L. Delavallée, P. Galán-Malo, M.E. Gilles, M.N. Brunelle-Navas, S.A. Susin, AIF-mediated caspase-independent necroptosis requires ATM and DNA-PK-induced histone H2AX Ser139 phosphorylation, Cell Death Dis. 3 (2012) e390.
[11] B. Lu, X. Gong, Z.Q. Wang, Y. Ding, C. Wang, T.F. Luo, M.H. Piao, F.K. Meng, G.F. Chi, Y.N. Luo, P.F. Ge, Shikonin induces glioma cell necroptosis in vitro by ROS overproduction and promoting RIP1/RIP3 necrosome formation, Acta Pharmacol. Sin. 38 (2017) 1543–1553.
[12] Z. Fu, B. Deng, Y. Liao, L. Shan, F. Yin, Z. Wang, H. Zeng, D. Zuo, Y. Hua, Z. Cai, The anti-tumor effect of shikonin on osteosarcoma by inducing RIP1 and RIP3 dependent necroptosis, BMC Canc. 13 (2013) 580.
[13] Z. Shahsavari, F. Karami-Tehrani, S. Salami, Shikonin induced necroptosis via reactive oxygen species in the T-47D breast cancer cell line, Asian Pac. J. Cancer Prev. APJCP 16 (2015) 7261–7266.
[14] J.I. Kang, J.Y. Hong, J.S. Choi, S.K. Lee, Columbianadin inhibits cell Proliferation by inducing apoptosis and necroptosis in HCT116 colon cancer cells, Biomol. Ther. (Seoul) 24 (2016) 320–327.
[15] N. Wada, Y. Kawano, S. Fujiwara, Y. Kikukawa, Y. Okuno, M. Tasaki, M. Ueda, Y. Ando, K. Yoshinaga, M. Ri, S. Iida, T. Nakashima, Y. Shiotsu, H. Mitsuya, H. Hata, Shikonin, dually functions as a proteasome inhibitor and a necroptosis inducer in multiple myeloma cells, Int. J. Oncol. 46 (2015) 963–972.
[16] C. Huang, Y. Luo, J. Zhao, F. Yang, H. Zhao, W. Fan, P. Ge, Shikonin kills glioma cells through necroptosis mediated by RIP-1, PLoS One 8 (2013) e66326.
[17] Z. Zhou, B. Lu, C. Wang, Z. Wang, T. Luo, M. Piao, F. Meng, G. Chi, Y. Luo, P. Ge, RIP1 and RIP3 contribute to shikonin-induced DNA double-strand breaks in glioma cells via increase of intracellular reactive oxygen species, Cancer Lett. 390 (2017) 77–90.
[18] P.Y. Lee, J. Costumbrado, C.Y. Hsu, Y.H. Kim, Agarose gel electrophoresis for the separation of DNA fragments, J. Vis. Exp. 2012 (2012) 62.
[19] M.W. Luczak, A. Zhitkovich, Monoubiquitinated γ-H2AX, Abundant product and

specific biomarker for non-apoptotic DNA double-strand breaks, Toxicol. Appl. Pharmacol. 355 (2018) 238–246.
[20] E. Daugas, S.A. Susin, N. Zamzami, K.F. Ferri, T. Irinopoulou, N. Larochette, M.C. Prévost, B. Leber, D. Andrews, J. Penninger, G. Kroemer, Mitochondrio-nuclear translocation of AIF in apoptosis and necrosis, FASEB J. 15 (2000) 729–739.
[21] A.A. Fatokun, V.L. Dawson, T.M. Dawson, Parthanatos: mitochondrial-linked mechanisms and therapeutic opportunities, Br. J. Pharmacol. 171 (2014) 2000–2016.
[22] D.M. Moquin, T. McQuade, F.K. Chan, CYLD deubiquitinates RIP1 in the TNFα-induced necrosome to facilitate kinase activation and programmed necrosis, PLoS One 8 (2013) e76841.
[23] D. Chen, J. Yu, L. Zhang, Necroptosis: an alternative cell death program defending against cancer, Biochim. Biophys. Acta 1865 (2016) 228–236.
[24] Y. Higuchi Y, Glutathione depletion-induced chromosomal DNA fragmentation associated with apoptosis and necrosis, J. Cell Mol. Med. 8 (2004) 455–464.
[25] Y. Higuchi Y, Chromosomal DNA fragmentation in apoptosis and necrosis induced by oxidative stress, Biochem. Pharmacol. 66 (2003) 1527–1535.
[26] M. Napirei, A.G. Basnakian, E.O. Apostolov, H.G. Mannherz, Deoxyribonuclease 1 aggravates acetaminophen-induced liver necrosis in male CD-1 mice, Hepatology 43 (2006) 297–305.
[27] R. Mizuta, S. Araki, M. Furukawa, Y. Furukawa, S. Ebara, D. Shiokawa, K. Hayashi, S. Tanuma, D. Kitamura, DNase γ is the effector endonuclease for internucleosomal DNA fragmentation in necrosis, PLoS One 8 (2013) e80223.
[28] C. Candé, N. Vahsen, I. Kouranti, E. Schmitt, E. Daugas, C. Spahr, J. Luban, R.T. Kroemer, F. Giordanetto, C. Garrido, J.M. Penninger, G. Kroemer, AIF and cyclophilin A cooperate in apoptosis-associated chromatinolysis, Oncogene 23 (2004) 1514–1521.
[29] Y. Wang, R. An, G.K. Umanah, H. Park, K. Nambiar, S.M. Eacker, B. Kim, L. Bao, M.M. Harraz, C. Chang, R. Chen, et al., A nuclease that mediates cell death induced by DNA damage and poly(ADP-ribose) polymerase-1, Science 354 (2016) 6308.
[30] B. Lu, Z. Wang, Y. Ding, X. Wang, S. Lu, C. Wang, C. He, M. Piao, G. Chi, Y. Luo, P. Ge, RIP1 and RIP3 contribute to shikonin-induced glycolysis suppression in glioma cells via increase of intracellular hydrogen peroxide, Cancer Lett. 425 (2018) 31–42.
[31] J. Chen, J. Xie, Z. Xiang, B. Wang, Y. Wang, X. Hu, Shikonin and its analogs inhibit cancer cell glycolysis by targeting tumor pyruvate kinase-M2, Oncogene 30 (2011) 4297–4306.
[32] H. Li, G. Chen, W. Ma, P.A. Li, Water-soluble coenzyme q10 inhibits nuclear translocation of apoptosis inducing factor and cell death caused by mitochondrial complex I inhibition, Int. J. Mol. Sci. 15 (2014) 13388–13400.
[33] Y. Hong, H. Nie, X. Wei, S. Fu, W. Ying, NAD+ treatment can prevent rotenone-induced increases in DNA damage, Bax levels and nuclear translocation of apoptosis-inducing factor in differentiated PC12 cells, Neurochem. Res. 40 (2015) 837–842.
[34] L. Zheng, C. Wang, T. Luo, B. Lu, H. Ma, Z. Zhou, D. Zhu, G. Chi, P. Ge, Y. Luo, JNK activation contributes to oxidative stress-induced parthanatos in glioma cells via increase of intracellular ROS production, Mol. Neurobiol. 54 (2017) 3492–3505.
[35] E.P. Rogakou, D.R. Pilch, A.H. Orr, V.S. Ivanova, W.M. Bonner, DNA double-stranded breaks induce histone H2AX phosphorylation on serine 139, J. Biol. Chem. 273 (1998) 5858–5868.
[36] J.T. Yang, Z.L. Li, J.Y. Wu, F.J. Lu, C.H. Chen, An oxidative stress mechanism of shikonin in human glioma cells, PLoS One 9 (2014) e94180.
[37] J. Zhao, S. Jitkaew, Z. Cai, S. Choksi, Q. Li, J. Luo, Z.G. Liu, Mixed lineage kinase domain-like is a key receptor interacting protein 3 downstream component of TNF-induced necrosis, Proc. Natl. Acad. Sci. U. S. A. 109 (2012) 5322–5327.
[38] B. Schenk, S. Fulda, Reactive oxygen species regulate Smac mimetic/TNFα- induced necroptotic signaling and cell death, Oncogene 34 (2015) 5796–5806.
[39] H. Wang, L. Sun, L. Su, J. Rizo, L. Liu, L.F. Wang, F.S. Wang, X. Wang, Mixed lineage kinase domain-like protein MLKL causes necrotic membrane disruption upon phosphorylation by RIP3, Mol. Cell 54 (2014) 133–146.
[40] A. Tocchi, E.K. Quarles, N. Basisty, L. Gitari, P.S. Rabinovitch, Mitochondrial dysfunction in cardiac aging, Biochim. Biophys. Acta 1847 (2015) 1424–1433.
[41] J. Zhang, Y. Yang, W. He, L. Sun, Necrosome core machinery: MLKL, Cell. Mol. Life Sci. 73 (2016) 2153–2163.
[42] Z. Fu, B. Deng, Y. Liao, L. Shan, F. Yin, Z. Wang, H. Zeng, D. Zuo, Y. Hua, Z. Cai, The anti-tumor effect of shikonin on osteosarcoma by inducing RIP1 and RIP3 dependent necroptosis, BMC Canc. 13 (2013) 580.
[43] C. Chen, W. Xiao, L. Huang, G. Yu, J. Ni, L. Yang, R. Wan, G. Hu, Shikonin induces apoptosis and necroptosis in pancreatic cancer via regulating the expression of RIP1/RIP3 and synergizes the activity of gemcitabine, Am. J. Transl. Res. 9 (2017) 5507–5517.
[44] Y. Qu, J. Shi, Y. Tang, F. Zhao, S. Li, J. Meng, J. Tang, X. Lin, X. Peng, D. Mu, MLKL inhibition attenuates hypoxia-ischemia induced neuronal damage in developing brain, Exp. Neurol. 279 (2016) 223–231.
[45] L. Zhao, H. Lin, S. Chen, S. Chen, M. Cui, D. Shi, B. Wang, K. Ma, Z. Shao, Hydrogen peroxide induces programmed necrosis in rat nucleus pulposus cells through the RIP1/RIP3-PARP-AIF pathway, J. Orthop. Res. 36 (2018) 1269–1282.
[46] C.Y. Huang, W.T. Kuo, Y.C. Huang, T.C. Lee, L.C. Yu, Resistance to hypoxia-induced necroptosis is conferred by glycolytic pyruvate scavenging of mitochondrial superoxide in colorectal cancer cells, Cell Death Dis. 4 (2013) e622.